Numerical Study of Transition Process in a Separated Boundary Layer on a Flat Plate with Two Different Leading Edges

ZHIYIN YANG
Department of Aeronautical and Automotive Engineering
Loughborough University
Loughborough LE11 3TU
UNITED KINGDOM
Z.Yang@lboro.ac.uk

Abstract: Transition from laminar flow to turbulent flow occurs very often and plays a crucial role in many practical engineering flows. There are many different kinds of transition and broadly speaking they can be classified into three categories: classical transition in attached boundary; bypass transition in attached boundary layer and separated boundary layer transition. This paper presents a comparative study of separated boundary layer transition on a flat plate with a blunt/semi-circular leading edge.

Boundary layer may separate due to an adverse pressure gradient or due to flow geometry. In the current study the geometry is a flat plate with two different leading edges: a blunt one and a semi-circular one. The main purpose of the study is to identify how similar or how different the transition process is with two different leading edges. This study shows that for both cases (blunt and semi-circular leading edges) the primary two-dimensional instability originates from the free shear layer of the separation bubble via the Kelvin-Helmholtz mechanism. Three-dimensional motions develop under any small spanwise disturbances and similar coherent structures have been observed from flow visualization in both cases, strongly indicating that the transition process is very similar.

Key-Words: Large-Eddy Simulation (LES); transition process; free shear layer; instability

1 Introduction

Transition from laminar boundary layer flow to turbulent boundary layer flow occurs in a wide range of practical engineering applications. The transition process has a great influence on the flow development downstream and it is very important to have a good understanding of the flow physics involved in order to predict it accurately, and to control it when needed. However, our current understanding of transition is far from complete, especially for separated boundary layer transition where the instability usually initiates from the free shear layer of a separation bubble.

Boundary layer may separate due to either an adverse pressure gradient such as aerofoil flow or due to flow geometry such as flows over vehicles, humps and other forms of localized surface curvature variations. Even at relatively low Reynolds numbers free shear layer in a separated laminar boundary layer may become inviscidly unstable and hence it undergoes a transition to turbulence. It is usually difficult to study it either experimentally (limited temporal and spatial resolution of flow parameters and hence a thorough description of the transition process is very hard) or theoretically (limitation imposed by nonlinearity of the transition process at later stages). It is also extremely hard, if not impossible, to study and predict the transition process accurately employing the conventional Reynolds-Averaged-Navier-Stokes (RANS) approach with several different methods since it only predicts the time- or ensemble-averaged flow field [1]. An alternative approach is called Large-Eddy Simulation (LES) first proposed by Smagorinsky [2] which computes large scale motions (large eddies) of transitional/turbulent flow directly and only small scale motions, called Sub-Grid Scale (SGS), are modelled whereas in the RANS approach all scale motions are modelled. Hence LES is more accurate than the RANS approach and computationally much cheaper than another approach called Direct Numerical Simulation (DNS) which computes fluid motions at all scales down to the smallest scale using very fine mesh. DNS is far too expensive for any practical engineering calculations and only used as a research tool for low Reynolds number flows.

Flow separation triggered by a blunt leading edge occurs in many practical situations such as flow over vehicles and flow over buildings while in many other cases flow separation is triggered by a smooth leading edge such as flow over aircraft wings and

flow over compressor/turbine blades. Many studies, both experimentally and numerically, have been carried out on blunt leading edge separation flows [3, 4, 5, 6, 7, 8] and smooth leading edge separation flows [9, 10, 11]. It is reasonably well understood for a bluff body that smooth edges could improve the aerodynamics characteristic of the body. However, it is not clear how different or similar the transition process could be with different leading edges. This paper presents a numerical study of the transition process in a separated boundary layer on a flat plate with two different leading edges (blunt and semi-circular) using LES.

2 Mathematical Formulation

2.1 Governing Equations

The governing equations for any fluid flow can be derived from the fundamental conservation laws for mass, momentum and energy. Generally speaking those conservation equations are three dimensional and time dependent, and may take different mathematical forms depending on the co-ordinates used. In LES only large eddies (large scale motions) are computed directly and hence a so called low-pass spatial filter is applied to the instantaneous conservation equations to formulate the 3D unsteady governing LES equations. When the finite volume method is employed the equations are integrated over control volumes, equivalent to convolution with a top-hat filter, hence there is no need to apply a filter to the instantaneous equations explicitly and in this case it is called implicit filtering. The governing LES equations are fairly standard and can be found in many text books [12, 13, 14] and papers [15, 16, 17, 18] so that they will only be very briefly presented here.

The governing LES equations expressing conservation of mass and momentum in a Newtonian incompressible flow in Cartesian form can be written as

$$\partial_i \overline{u_i} = 0 \tag{1}$$

$$\partial_t(\overline{u}_i) + \partial_j(\overline{u}_i\overline{u}_j) = -\frac{1}{\rho}\partial_i \overline{P} + 2\partial_j(\nu_{eff}\,\overline{s_{ij}}) \tag{2}$$

where the bar over the variables denotes the filtered, or resolved scale quantity and it should be noted that a modified pressure, $\overline{P} = \overline{p} + \frac{1}{3}\tau_{ll}$, has been introduced and hence when the above equation is solved the pressure obtained is not just the static pressure only. ν_{eff} is the effective viscosity (molecular viscosity + SGS viscosity) and $\overline{s_{ij}}$ is

$$\overline{s_{ij}} = \frac{1}{2}(\partial_i \overline{u_j} + \partial_j \overline{u_i}) \tag{3}$$

The SGS viscosity needs to be calculated from a SGS model [19, 20] and the most basic model is the one originally proposed by Smagorinsky [2]:

$$\mu_t = \rho(C_S\overline{\Delta})^2 S \qquad S = (2\overline{S_{ij}}\,\overline{S_{ij}})^{\frac{1}{2}} \qquad \Delta = (\Delta x\Delta y\Delta z)^{\frac{1}{3}} \tag{4}$$

C_S is the Smagorimsky constant and typical value used for it is 0.1. This simple model has been used widely and proved surprisingly successful although it has clear shortcomings such as that it is too dissipative and the Smagorinsky constant should be different for different flows. One way to improve this simple SGS model was proposed by Germano, Piomelli, Moin and Cabot [21] – a dynamic SGS model, which allows the model constants C_S to be determined locally in space and in time during the simulation. Generally speaking if the mesh is fine in LES then SGS models may not play an important role at all as most of the turbulent motions will be computed directly. However, Reynolds number in representative engineering flows is usually quite high and hence it would be very expensive if a fine mesh is used, or when very fine mesh cannot be afforded. Therefore the SGS modelling of small-scale turbulence is of primary importance in LES for industrial flows, especially at high Reynolds numbers when relatively coarse grids are being used. Unfortunately all current available SGS models are not satisfactory when coarse mesh is used in LES so that it is highly necessary to develop advanced SGS models that are capable of handling practical engineering turbulent flow at high Reynolds numbers.

The Poisson equation for pressure can be derived by taking the divergence of (2)

$$\partial_i\partial_t(\overline{u_i}) + \partial_i\partial_j(\overline{u}_i\overline{u}_j) = -\partial_i\partial_i\overline{p} + 2\partial_i\partial_j(\nu_{eff}\,\overline{S_{ij}}) \tag{5}$$

and using equation (1) one finally obtains

$$\partial_i\partial_j\overline{p} = \Delta^2\overline{p} = \partial_i H_i \tag{6}$$

where

$$H_i = \partial_j(-\overline{u}_i\overline{u}_j + 2\nu_{eff}\overline{S_{ij}}) \quad (7)$$

It is computationally very expensive to solve equation (6) for 3D high Reynolds flows and one way to speed up the solution is to Fourier transform the equation in z direction to obtain a set of decoupled 2D equations:

$$\frac{\partial^2\tilde{p}}{\partial^2 x} + \frac{\partial^2\tilde{p}}{\partial^2 y} - k_z^2\tilde{p} = \tilde{R} \quad (8)$$

Provided flow is homogeneous in z direction so that a periodic boundary condition can be applied. k_z is the discrete Fourier wave number given as

$$k_z = \frac{2\sin(k_z/2)}{\Delta z} \quad (9)$$

The two-dimensional equation (8), one for each value of k_z can be solved very quickly even when the geometry is complex as long as flow is homogeneous in z direction.

2.2 Numerical Method

The numerical method used in the present study is direct descendant of well-known finite-volume techniques successfully used for many high-Reynolds-number LES studies. A standard dynamic SGS model is used to approximate the unknown SGS stresses. The explicit second order Adams-Bashforth scheme is used for temporal discretisation and the spatial discretisation is the second-order central differencing which is widely used in LES owing to its non-dissipative and conservative properties. The Poisson equation for pressure is solved using an efficient hybrid Fourier multi-grid method. Details of the numerical method and the dynamic subgrid-scale model have been reported elsewhere by Yang & Voke [9, 17].

2.3 Computational Details

Two numerical simulations of separated boundary layer transition under zero free stream turbulence on a flat plate have been performed, one with a blunt leading edge and the other one with a smooth semi-circular leading edge. Figure 1 shows the computational domain and mesh.

For the semi-circular leading edge case, the circular inflow boundary and the lateral boundaries are 8H distant from the surface, corresponding to a blockage ratio of 16, H is the plate thickness, also equal to the diameter of the leading edge circular diameter (0.01m). A free-slip but impermeable boundary is applied on the lateral boundaries. On the outflow boundaries, 9.5H downstream of the leading edge, a convective boundary condition is applied. The spanwise dimension of the domain is 4H and a periodic boundary condition is applied in this direction. The mesh points are 408 (streamwise, wrapped round the leading edge) by 72 (wall-normal, clustered in the near wall region) and by 64 (spanwise). The inflow velocity U_0 is uniform and aligned with the plate. The Reynolds number based on the inflow velocity and the plate leading-edge diameter is 3450. In terms of wall units based on the shear layer downstream of reattachment at x/x_R = 2.5 (x_R is the mean separation bubble length), the streamwise mesh sizes vary from $\Delta x+ = 10$ to 30.5, $\Delta z+$ is about 20, nearest to the wall the minimum $\Delta y+ = 1$ so that no-slip wall boundary condition is directly applied at the plate surface without the need of wall functions and the maximum $\Delta y+ = 90$. The time step used in the simulation is $0.005H/U_0$. Statistics were gathered by averaging in time once the simulation reached a statistically stationary state and also over the span direction and on both sides of the plate. The simulation was run initially for 40,000 time steps to allow the transition and turbulent boundary layer to become established, and the mean quantities were then gathered over a further 60,000 steps with a sample taken every 20 time steps (3,000 samples).

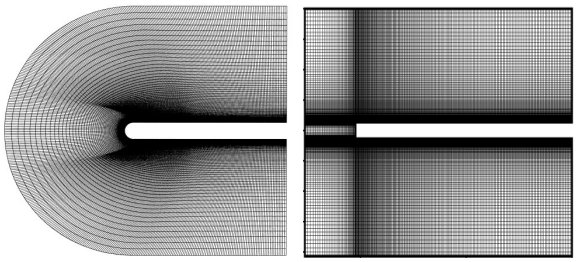

Fig. 1 computational domain and mesh.

For the blunt leading edge case, the computational domain is 25H along the x direction (streamwise), 16H in the y direction (normal) and 4H in the z direction (spanwise), H is the plate thickness and is the same as in the semi-circular leading edge case (0.01m). The inflow boundary is 5H from the leading edge whereas the outflow boundary is 20H downstream the leading edge. The lateral boundaries are at 8H from the surface, corresponding to a blockage ratio of 16 which is the same as in the semi-circular leading edge case. The

mesh points are 256 along the x direction, 212 in the y direction and 64 in the z direction. In terms of wall units based on the friction velocity downstream of reattachment at $x/x_R = 2.5$, the streamwise mesh sizes vary from $\Delta x+ = 9.7$ to 48.5, $\Delta z+$ is around 20 and nearest to the wall the minimum $\Delta y+ = 2$ and the maximum $\Delta y+ = 50$. The Reynolds number based on the inflow velocity and plate thickness is 6500 and the time step used in the simulation is $0.001885H/U_0$. Similar boundary conditions as in the semi-circular leading edge case are employed. The simulation initially was run for 70,000 time steps to allow the transition and turbulent boundary layer to become established, and the averaged results were then gathered over a further 399,000 steps with a sample taken every 10 time steps (39,900 samples) and averaged over the spanwise direction too.

3 Results and Discussion

3.1 Mean variables

One of the most important parameter characterizing a separated/reattached flow is the time mean position of the reattachment, i.e. time-averaged separation bubble length so that it is important to calculate it accurately. Usually there are four methods to determine the mean reattachment point, i.e., (a) by the location at which the mean velocity is zero at the first grid point away from the wall or where velocity changes from negative to positive; (b) by the location of zero wall-shear stress; (c) by the location of the mean dividing streamline; (d) by a p.d.f method in which the mean reattachment point is indicated by the location of 50% forward flow fraction. The first three methods have been found usually to give the reattachment point within 0.1% difference, and are about 2% different for the p.d.f results. In the present study the first method was used and for the semi-circular leading edge case the simulated mean separation bubble length is about 2.6H (H is the plate thickness, the same as the leading edge diameter) and the measured mean bubble length is about 2.75H. The simulated mean bubble length agrees well with the experimental one and the small discrepancy is likely due to different blockage ratios (blockage ratio of the experiment is about twice that of the simulation). For the blunt leading edge case the measured mean bubble length is about 7.7H (H is the plate thickness) while the simulated one is about 6.5H. A reasonably good agreement is also obtained and again the discrepancy is mainly due to different blockage ratios (blockage ratio of the experiment in this case is about 4 times that of the simulation). It also worth pointing out that the mean separation bubble length is much larger in the blunt leading edge case which is understandable as the flow in this case is forced to turn almost 90^0 from horizontal direction to vertical direction at the leading edge, leading to a much bigger separation bubble.

The predicted mean velocity and turbulence quantities compare well with the corresponding experimental data in both cases, especially for the smooth leading edge case. Figures 2(a) and 2(b) show the mean and r.m.s. fluctuating parts of the streamwise velocity compared with experiment (Coupland, private communication) at seven streamwise stations for the smooth leading edge case. The profiles are plotted as functions of y/x_R at corresponding values of x/x_R. As can be seen from figure 2(*a*) excellent agreement between the experimental data and the simulated results has been obtained for the mean streamwise velocity profiles. Differences in the free stream arise entirely from the differences in the blockage ratio. The agreement for the r.m.s. fluctuations, as shown in figure 2(*b*), is also good, except that the simulation shows higher peaks of u' occurring closer to the wall at two stations in the bubble, especially at $x/x_R = 0.66$ where the discrepancy between the peak values is about 25%, but lack of experimental data (taken with a single hot-wire probe) in the near wall region makes detailed comparisons difficult. After the reattachment, the agreement is much better.

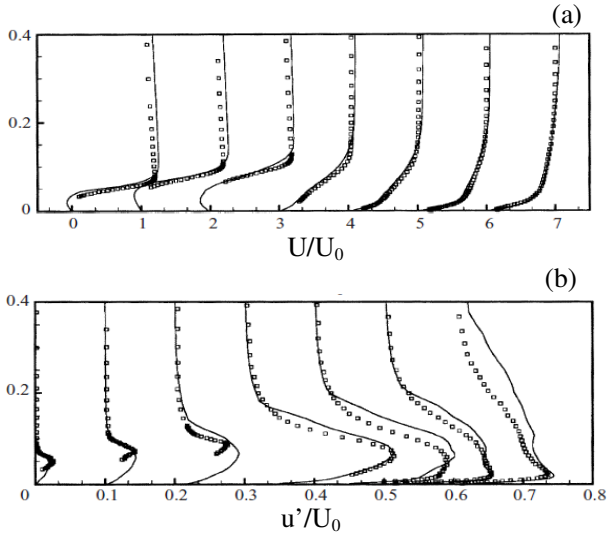

Fig. 2 Mean axial velocity and r.m.s profiles at seven axial locations measured from the blend point for the smooth leading edge case. Left to right, $x/x_R = 0.22, 0.44, 0.66, 1.09, 1.64, 2.55$. Solid line, LES; symbols, experimental data.

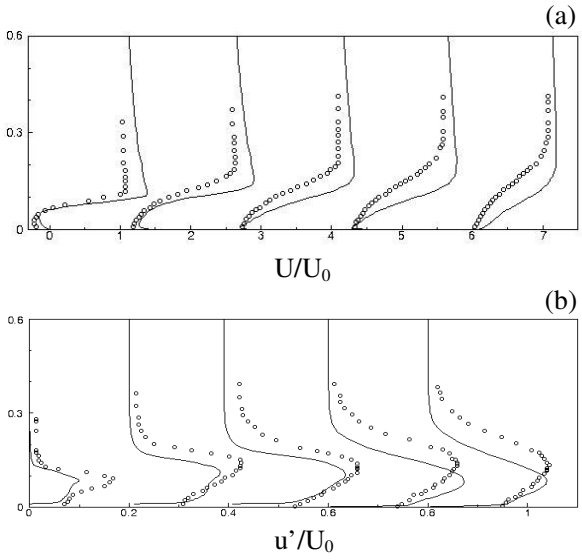

Fig. 3 Mean axial velocity and r.m.s profiles at five axial locations measured from the leading edge for the blunt leading edge case. Left to right, x/x_R = 0.2, 0.4, 0.6, 0.8, 1.0. Solid line, LES; symbols, experimental data.

Figures 3(a) and 3(b) show the comparison between the predicted mean streamwise velocity and r.m.s profiles and the experimental data [3] at five streamwise locations for the blunt leading edge case. The profiles are plotted as functions of y/x_R at corresponding values of x/x_R, with the velocity and r.m.s values normalised by the free stream velocity. The experiment was carried out at a higher Reynolds number (26,000) and hence the flow was turbulent rather than transitional in the experiment. The LES results show a reasonably good agreement with the experimental data, not as good as for the smooth leading edge case. The predicted peak and the free stream values of the velocity are bigger than those measured whereas the r.m.s values at the first two stations are smaller. Those discrepancies are due to the differences in blockage ratio (nearly 4 times in the experiment as in the current study), due to the Reynolds number differences (26,000 in the experiment and 6500 in the current study) and maybe mainly due to the fact that it was turbulent separation at the leading edge in the experiment while it is laminar separation in the current study.

3.2 Transition Process

The transition process can be clearly seen from figure 4 which shows two snapshots (one for the semi-circular leading edge case and the other one for the blunt leading edge case) of instantaneous spanwise vorticity in the (x, y) plane at the mid-span location (it looks very similar at different spanwise locations). Snapshots at other times are also very similar and hence will not be presented. It is evident that transition processes are very similar for both cases and it occurs earlier in the blunt leading edge case. At early stage of the separation bubble a steady free shear layer develops associated with formation of two-dimensional spanwise vortices; the free shear layer is inviscidly unstable and any small disturbances present grow downstream causing the deformation and distortion of the initial two-dimensional spanwise vortices. Further downstream those two-dimensional vortices become more distorted and deformed, and roll up leading to streamwise vorticity formation associated with significant three-dimensional motions, eventually breaking down at about the reattachment point and developing rapidly into a turbulent boundary layer. This process can be seen more clearly in figure 7 which shows three-dimensional coherent structures. Again it can be seen clearly that transition processes in both cases are very similar with almost identical coherent structures: two-dimensional vortices, usually called Kelvin-Helmholtz vortices or billows, at early stage and three-dimensional vortical structures called hairpin or Λ-shaped vortices further downstream before breaking down to small scale turbulence.

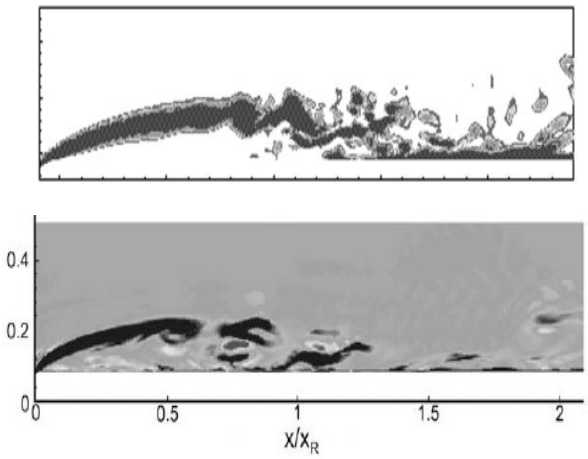

Fig. 4 Instantaneous spanwise vorticity in the (x, y) plane, above: smooth leading edge; below: blunt leading edge.

It is clear from the above discussion that qualitatively the transition processes in both cases are very similar and the free shear layer becomes unstable via an inviscid instability which is most likely the Kelvin-Helmholtz instability. Detailed

quantitative analysis will be carried out here to clarify this point.

3.3 Instability of the Free Shear Layer

The Kelvin-Helmholtz instability was originally derived from two parallel stream of fluids with different velocity and density. Hence there are discontinuities in density and velocity at the interface. Chandrasekhar [22] considered the case of continuous variation of velocity and certain distribution of ρ (characterized by the Richardson number) and concluded from the inviscid linear stability analysis that, for any values of the Richardson number, there are always bands of wavelengths for which the Kelvin-Helmholtz instability occurs. In particular, when the Richardson number is zero, i.e. for constant density, the condition for the Kelvin-Helmholtz instability to occur is $0 < Kh < 1.2785$ where K is the wave number and h is the shear layer thickness. Both K and h can be extracted from LES data in the present study and for the semi-circular leading edge case Kh = 0.984 and for the blunt leading case Kh = 1.1245 (h is the shear layer thickness where the unsteadiness first becomes apparent and $K = 2\pi f/c$, f is the characteristic frequency which is obtained from the spectra analysis as shown in figure 5 and c is the wave speed equal to the velocity at the critical layer, i.e., the streamwise velocity at the inflection point). Hence it can be concluded that the free shear layer in both cases becomes unstable via the same instability, Kelvin-Helmholtz instability.

3.4 Vortex Shedding

It has been evident from experimental studies [3, 4, 5] that separated-reattached flows in a blunt leading edge are associated with vortex shedding and the measured average shedding frequency is about $0.6 - 0.7U_0/x_R$ (U_0 is the free stream velocity and x_R is the mean separation bubble length). In addition, there is a low frequency peak according to the experimental data. Figure 5 presents the velocity spectra for the semi-circular leading edge and the blunt leading edge cases and it can be seen clearly that there is a peak band of frequencies for both cases, not periodic in the sense that there is only a single frequency. The shedding process occurs within a narrow band of frequencies and for the semi-circular leading edge case the predicted average frequency can be estimated at about $0.74U_0/x_R$. For the blunt leading edge case the predicted average frequency is about $0.78U_0/x_R$, both values are close to the experimental data, indicating that the simulations capture the flow physics of vortex shedding well and also confirm that the shedding process in both cases are very similar. The low frequency peak observed in many experimental studies are not apparent in the present study although in the semi-circular leading edge case a low frequency peak band was visible further upstream as shown in figure 6 and an explanation was given regarding how it happens [9]. However, this low frequency has not been observed in the LES studies for the blunt leading edge case [7, 8] and further investigation is needed in this area to fully understand this phenomenon.

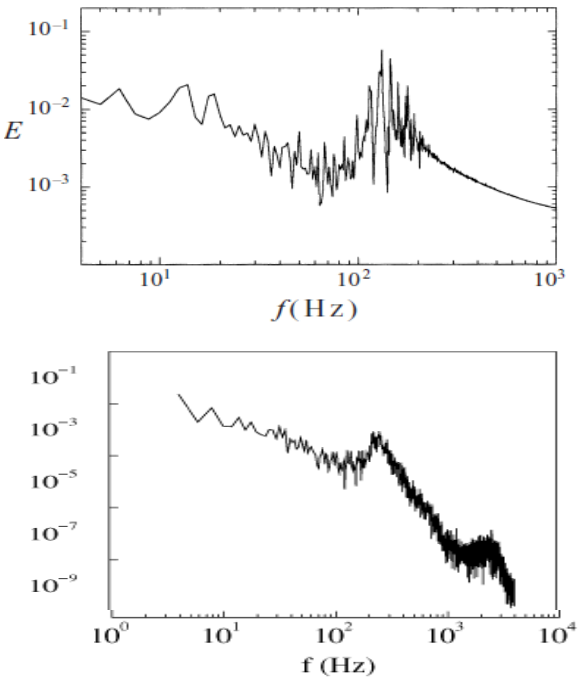

Fig. 5 Velocity spectra, above: semi-circular leading edge at $x/x_R = 0.7$ and $y/x_R = 0.04$; below: blunt leading edge at $x/x_R = 0.5$ and $y/x_R = 0.13$.

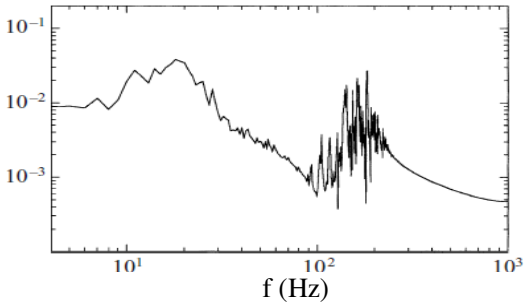

Fig. 6 Power spectrum of u' at $x/x_R = 0.35$ and $y/x_R = 0.04$ for the semi-circular leading edge case.

3.5 Large-Scale Vortex Structures

It has been well established that large scale structures, usually called coherent structures, exist in many transitional and turbulent flows. The topology and range of scales of those large scale structures vary from flow to flow such as counter-rotating vortices in wake flows, streaks and hairpin vortices in turbulent boundary layer. In the present study the flow visualisation reveals various kinds of large scale 2D and 3D structures as shown in figure 7.

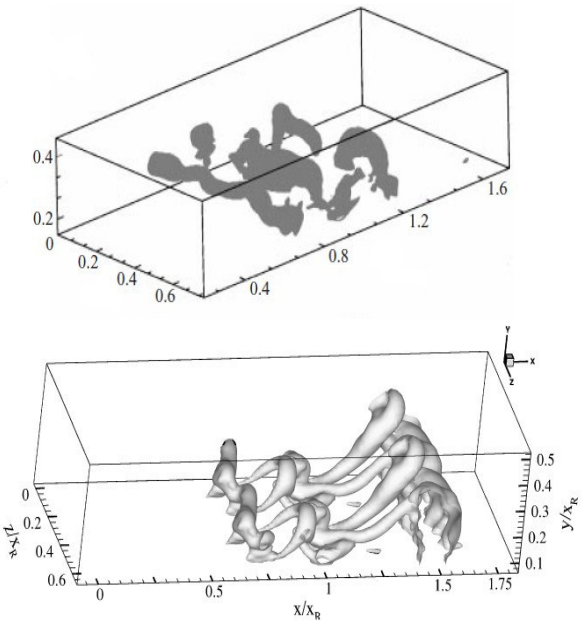

Fig. 7 Low-pressure iso-surfaces showing the transformation of Kelvin-Helmholtz rolls into hairpin or Λ-shaped vortices, above: semi-circular leading edge; below: blunt leading edge.

The free shear layer becomes unstable due to Kelvin-Helmholtz instability and the two-dimensional Kelvin-Helmholtz rolls are shed downstream of the plate leading edge and become distorted as they travel downstream. The Kelvin-Helmholtz rolls are subjected to approximately sinusoidal undulation (waviness) along the spanwise. It can clearly be seen that the axis of the the spanwise rolls remains perpendicular to the flow direction thus keeping their coherency and two-dimensionality nature up to a certain distance downstream. Further downstream the above described 2D spanwise coherent vortical structures become more distorted (specially the initially shed roll) leading to the appearance of a well-organised array of streamwise vortices originating from the initially shed vortical tube, and transform into three-dimensional vortical structures called Λ-vortices as shown in figure 7. This process is quite similar in both cases.

The 2D Kelvin-Helmholtz rolls can be transformed into 3D vortical structures called Λ-vortices as shown in figure 7. However it is also possible that those 2D rolls can be transformed into another form of 3D vortical structures called ribs [23] as shown in figure 8 below. It can be seen from these figures that the Kelvin-Helmholtz rolls have been transformed into streamwise ribs connecting a totally distorted and torn apart spanwise vortical structures. It is quite tempting to assume that these ribs are actually originating from Lambda-shaped vortices which are subjected to more stretching along the axial direction leading to the disintegration of its legs.

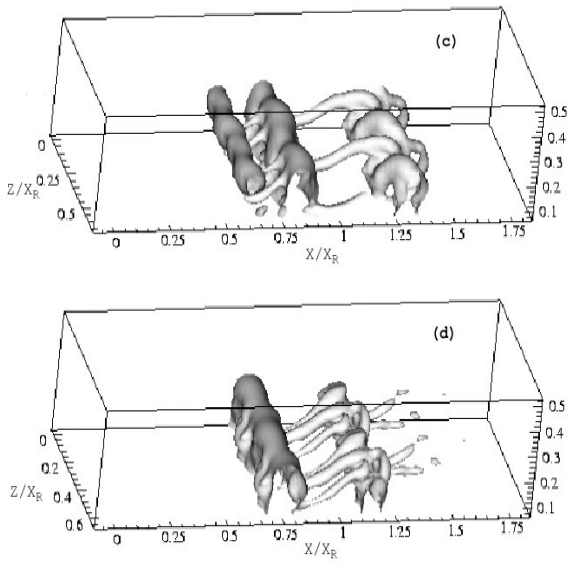

Fig. 8 Low-pressure iso-surfaces displaying the transformation of 2D Kelvin-Helmholtz rolls into streamwise large-scale vortical structures called ribs for the blunt leading edge case.

The transition process is usually very complicated and can follow many possible routes. For attached boundary layer transition the transition process can be divided into the following several stages [24]:

1). Receptivity stage – how the disturbances are projected into growing eigenmodes, or how they enter or otherwise induce disturbances in a boundary layer.

2). Linear growth stage (primary instability) – small disturbances are amplified till they reach a size where nonlinear growth starts. This amplification can be in the form of exponential

growth of eigenmodes, nonmodal growth of optimal disturbances, or nonmodal responses to forcing.

3). Secondary instability – Usually once a disturbance reaches a finite amplitude it often saturates and transform the flow into a kind of new, possibly steady state. Very rarely the primary instability can lead the flow directly in a turbulent state and the new steady or quasi-steady flow becomes a base on which secondary instability can occur. This secondary instability can be viewed as a new instability of a more complicated flow.

4). The breakdown stage – nonlinearities and possibly higher instabilities excite an increasing number of scales and frequencies in the flow. This stage is more rapid than both the linear stage and the secondary instability stage.

However, for the separated boundary layer flow the transition process is less well understood compared with the attached boundary layer transition. It is proposed [6] that this transformation of the Kelvin-Helmholtz rolls into the three-dimensional vortical structures is likely due to a secondary instability, the helical pairing instability, which is a kind of two-dimensional subharmonic Eckhaus-type secondary instability [24]. The result is the growth of a disturbance with twice the wavelength of the initial vortices, producing a pairing of two vortices into a row of vortices, which can be seen from figure 9.

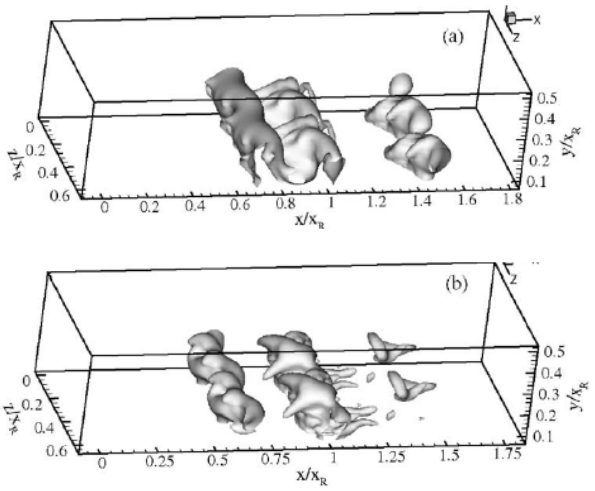

Fig. 9 Pairing of 2D Kelvin-Helmholtz rolls, indicating a kind of 2D subharmonic secondary instability for the blunt leading edge case.

Another possibility is that the 2D Kelvin-Helmholtz vortices can experience the so called three-dimensional elliptic-type secondary instability [24] and the result is the growth of spanwise disturbances on the 2D vortices in conjunction with the appearance of secondary streamwise vortices connecting the original spanwise vortices. Once the three-dimensional disturbance reaches a finite amplitude it leads to a bending of the core of the 2D vortices in the streamwise direction, eventually resulting in the so called rib vortices as shown in figure 8. It is not entirely clear which secondary instability is more dominant as both the pairing of vortices and the rib vortices have been observed in the present study, especially in the blunt leading edge case and further study is needed to clarify this point.

The breakdown stage occurs around the reattachment point and it happens rapidly as mentioned above, associated with irregular vortex shedding and the instantaneous reattachment point is moving upstream and downstream greatly. The instantaneous reattachment point can move about 50% of the mean bubble length. Immediately after the reattachment point a turbulent boundary layer forms quickly but it takes a quite long distance downstream for the log law and inner turbulence structures to develop as reported by many studies [25, 26, 27]. Since the final stage of breakdown is very complicated and involves strong nonlinearities and possibly higher instabilities so that both experimental and theoretical studies have their limitations and the most promising tools to study this is numerical simulations.

4 Conclusion

This paper presents a comparative study of transition process of a separated boundary layer on a flat plate with two different leading edges (blunt and semi-circular). The entire transition process, starting from initial instability in the free shear layer of the separation bubble and eventually leading to breakdown to turbulence has been visualized for both cases. It can be seen clearly that transition processes in both case are very similar with similar two-dimensional Kelvin-Helmholtz rolls and three-dimensional vortical structures (Λ-vortices) observed at various stages of the transition process in both cases. From detailed quantitative analysis of the LES data it has been shown that the free shear layer formed in the separation bubble is inviscidly unstable via the Kelvin-Helmholtz instability mechanism in both cases. These initial two-dimensional instability waves grow downstream linearly, with slow development of three-dimensional motions via possibly a secondary

instability mechanism responsive to any small spanwise disturbance. Further downstream the distorted spanwise two-dimensional vortices roll up, leading to the formation of three-dimensional vortical structures. Breakdown to turbulence occurs around the mean reattachment point and the flow develops into a turbulent boundary layer rapidly after the reattachment.

Similar vortex shedding from the separated free shear layer has been observed in both cases. This is not periodic in the sense that a unique frequency exists, and the predicted average characteristic shedding frequencies in both cases are close to the measured value indicating that the numerical simulations have captured the flow physics well. Nevertheless the low frequency peak observed in several experimental studies of separated flow over a blunt plate is not apparent in the simulations.

The transformation of two-dimensional Kelvin-Helmholtz rolls into three-dimensional vortical structures may be due to a secondary instability, a kind of two-dimensional subharmonic Eckhaus-type secondary instability or a three-dimensional elliptic-type secondary instability, and further studies are needed to clarify this. Other factors which can influence the transition process in a separated boundary layer such as free stream turbulence have not been discussed at all in the present paper. The final breakdown stage to turbulence is far from fully understood and further research in this area is much needed.

Acknowledgment: The author gratefully acknowledges that some of the results presented in this paper were produced by Dr. I.E. Abdalla during his Ph.D study under my supervision.

References:

[1] R.B. Langtry and F.R. Menter, Transition Modelling for General CFD Applications in Aeronautics, *AIAA 2005-522, Reno, Nevada*.

[2] J. Smagorinsky, General Circulation Experiments with the Primitive Equations: I – the Basic Experiment, *Monthly Weather Review*, Vol. 91, 1963, pp. 99-164.

[3] M. Kiya, K. Sasaki, Structure of a Turbulent Separation Bubble, *Journal of Fluid Mechanics*, Vol. 137, 1983, pp. 83-113.

[4] M. Kiya, K. Sasaki, Structure of Large-scale Votices and Unsteady Reverse Flow in the Reattaching Zone of a Turbulent Separation Bubble," *Journal of Fluid Mechanics*, Vol. 154, 1985, pp. 463-491.

[5] N. J. Cherry, R. Hillier, M. P. Latour, Unsteady Measurements in a Separated and Reattaching Flow, *Journal of Fluid Mechanics*, Vol. 144 1984, , pp. 13-46.

[6] I. E. Abdalla, Z. Yang, 'Numerical Study of the Instability Mechanism in Transitional Separating - Reattaching Flow, *International Journal of Heat and Fluid Flow*, Vol. 25, 2004, pp 593-605.

[7] I. E. Abdalla, Z. Yang, Numerical Study of a Separated-Reattached Flow on a Blunt Plate", *AIAA Journal*, Vol. 43, 2005, pp 2465-2474.

[8] Z. Yang, I. E. Abdalla, Effects of Free-Stream Turbulence on a Transitional-Reattached Flow over a Flat Plate with a Sharp Leading Edge," *International Journal of Heat and Fluid Flow*, Vol. 30, 2009, pp 1026-1035.

[9] Z. Yang, P. R. Voke, Large-eddy simulation of boundary layer separation and transition at a change of surface curvature, *Journal of Fluid Mechanics*, Vol. 439, 2001, pp. 305-333.

[10] V. S. Djanali, K.C. Wong, S.W. Armfield, Numerical Simulations of Transition and Separation on a Small Turbine Cascade, *WSEAS Transactions on Fluid Mechanics*, Vol. 1, 2006, pp. 879-884.

[11] M. Ubaldi, P. Zunino, Transition and Loss Generation in the Profile Boundary Layer of a Turbine Blade, *WSEAS Transactions on Fluid Mechanics*, Vol. 1, 2006, pp. 779-784.

[12] P. Sagaut, *Large Eddy Simulation for Incompressible Flows*, 2nd edition, Springer, 2002.

[13] M. Lesieur, O. Metais, P. Comte, *Large-Eddy Simulation of Turbulence,* Cambridge University Press, 2005.

[14] E. Garnier, P. Sagaut, N. Adams, *Large Eddy Simulation for Compressible Flows*, Springer, 2009.

[15] S. A. Jordan, Large-Eddy Simulation Methodology in Generalized Curvilinear Coordinates, *Journal of Computational Physics*, Vol. 148, 1999, pp. 322-340.

[16] Z. Yang, Large Eddy Simulation of Fully Developed Turbulent Flow in a Rotating Pipe, *International Journal for Numerical Methods in Fluids*, Vol. 33, 2000, pp. 681-694.

[17] Z. Yang, P. R. Voke, Large-Eddy Simulation of Separated Leading-Edge Flow in General Co-ordinates, *International Journal for Numerical Methods in Engineering*, Vol. 49, 2000, pp. 681-696.

[18] K. Mahesh, G. Constantinescu, P. Moin, A Numerical Method for Large-Eddy Simulation in Complex Geometries, *Journal of Computational Physics*, Vol. 197 2004, pp. 215-240.

[19] M. Lesieur, O. Metais, New Trends in Large Eddy Simulations of Turbulence, *Annual Review of Fluid Mechanic,* Vol. 28, 1996, pp. 45-82.

[20] T. Kajishima, T. Nomachi, One-Equation Sub-grid Scale Model Using Dynamic Procedure for the Energy Production, *Transaction of ASME*, Vol. 73, 2006, pp. 368-373.

[21] P. Germano, U. Piomelli, P. Moin, W. H. Cabot, A Dynamic Sub-grid Scale Eddy Viscosity Model, *Physics of Fluids,* Vol. 3, 1991, pp. 1760-1765.

[22] S. Chandrasekhar, *Hydrodynamic and Hydromagnetic Stability*, Clarendon, 1961.

[23] Z. Yang, I.E., Abdalla, On Coherent Structures in a Separated/Reattached Flow, *WSEAS Transactions on Fluid Mechanics*, Vol. 3, 2008, pp. 143-153.

[24] P.J. Schmid, D.S. Henningson, *Stability and Transition in Shear Flows*, Springer, 2001.

[25] P. Bradshaw, F.Y.F, Wong, 1972 The Reattachment and Relaxation of a Turbulent Shear Layer, *Journal of Fluid Mech*anics, Vol. 52, 1972, pp. 113-135.

[26] M. Alam, N.D. Sandham, Direct Numerical Simulation of `Short' Laminar Separation Bubbles with Turbulent Reattachment, *Journal of Fluid Mech*anics, Vol. 410, 2000, pp. 1-28.

[27] I. Castro, E. Epik, Boundary Layer Development after a Separated Region, *Journal of Fluid Mech*anics, Vol. 374, 1998, pp. 91-116.